buildings

MDPI

Article

The Partial Collapse of the South Road Axis Viaduct in Brasilia—A Forensic Investigation

Yuri Bessa Cesarino [1,*], José Melo [1], Humberto Varum [1] and Carlos Feijão [2]

[1] CONSTRUCT-LESE, Faculty of Engineering (FEUP), University of Porto, 4200-465 Porto, Portugal; josemelo@fe.up.pt (J.M.); hvarum@fe.up.pt (H.V.)
[2] Companhia Urbanizadora da Nova Capital do Brasil—NOVACAP, Setor de Áreas Públicas, Lote B, EPIA, SIA Sul, Brasília 71215-000, DF, Brazil; chlfeijao@gmail.com
* Correspondence: up202212113@fe.up.pt or bessayuri@gmail.com

Abstract

The partial collapse of the South Road Axis Viaduct in 2018 generated widespread concern about the safety of similar critical bridges and viaducts built during the same historical period in Brasilia. Since many of these structures were designed with analogous structural systems, a thorough post-incident investigation was conducted to understand the failure mechanisms involved. The viaduct collapse remains insufficiently examined in the available technical literature. The present work offers a detailed forensic investigation of the partial collapse of the asset, clarifying the key structural elements and governing mechanics that triggered the sudden failure. This study combined the collection of historical documentation, in situ debris investigation, geometrical and mechanical characterization, manual and numerical calculations, and the determination of structural performance. The results revealed that the viaduct had hidden vulnerabilities (such as a lack of structural redundancy and insufficient reinforcing steel) and significant material degradation and that it was operating under unpredicted high cyclic shear demands. Lastly, the repairs and strengthening techniques employed in the viaduct's recovery are also presented.

Keywords: prestressed concrete; bridges; sudden failure; retrofit; maintenance

1. Introduction

1.1. Brasilia Historical Context

Brasilia was the first planned Federal District of Brazil. The city was envisioned by the urban planner Lucio Costa and inspired by the architectural design of Oscar Niemeyer, while the landscape was designed by Roberto Burle Marx. Brasilia's origins date back to the 18th century, when the location was considered a possible route connecting the center of the country and as a means of protecting the administrative power from the vulnerable coastline. The city, however, was only planned in the mid-1950s by the administration of President Juscelino Kubitschek, who established an ambitious national modernization initiative to move the former capital from Rio de Janeiro to the center of the country.

The city's master plan, in fact, began to materialize only in 1956, and the construction of the new capital took, astonishingly, 41 months and was officially concluded in 1960. The city plan divided it into two major axes (the Monumental and Road Axes) that conveniently crossed at the city center. This design, combined with a smart multi-lane system with roundabouts and cloverleaf ramps, effectively increased mobility but required the city to have hundreds of these structures. Additionally, the robust design and monumental

Check for updates

Academic Editor: Fabrizio Gara

Received: 21 August 2026
Revised: 12 September 2026
Accepted: 18 September 2026
Published: 24 September 2026

character of the city required massive amounts of construction materials and a formidable workforce. During this period, large numbers of workers from across the country were mobilized for the construction of Brasilia, contributing to the city's unique social diversity. This period was also marked by the creation of the first public engineering company of the New Capital (NOVACAP), which represents a milestone in the local administrative workforce.

Today, Brasilia stands out for its iconic urban plan, characterized by curved concrete monuments that combine brutalist architectural identity with modernist philosophy. It is represented by functionality, rationality, zoning, open spaces, and a futuristic vision of progress. These singular features granted the city UNESCO World Heritage status in 1987 as a distinctive expression of modernist urban principles.

1.2. Rapid Growth and Unforeseen Traffic Demands in Brasilia

Originally, Brasilia was planned to house half a million people, and families were expected to own 1 vehicle each, which gives an estimate of the total number of vehicles of around 125 thousand for the whole city. However, due to its political significance and quality of life, Brasilia has become the third-largest city in the country, with a population of 3.5 million and about 5 million in the metropolitan area—almost 10 times larger than originally considered. This immense increase has imposed heavy demands on infrastructure, housing, and transportation.

The urban features of the city (large spaces, zoning, and wide roads) require the ownership of personal vehicles, creating a natural demand among city residents. In fact, data from the Department of Roads and Highways (DER/DF) [1] indicate an average of 120,000 vehicles per day crossing the capital via the main arterial roads (Monumental Axis and South Road Axis). This traffic demand is now greater than the city's original total vehicle population, as estimated in 1960.

1.3. Significance of the South Road Axis Viaduct's Partial Collapse

The sudden partial collapse of the South Road Axis Viaduct at the Galeria dos Estados (Figure 1) revealed structural vulnerabilities that could have been common to similar critical structures built during the same period of Brasilia's construction. This alarmed the authorities and the population, even more so after the temporary obstruction of one of the main arterial roads in the Federal District.

Figure 1. Section of the viaduct at Galeria dos Estados after the partial collapse in 2018, with indication of fracture of the main elements.

Historical records, however, confirm that the viaduct's deteriorating condition did not go entirely unnoticed. Visual inspections documented by Sinaenco (Architectural and Engineering Syndicate) in 2009 and 2011 cataloged visible degradation across the structure, resulting in formal requests to the relevant authorities for urgent maintenance involvements [2]. Yet, no public records of engineering interventions on this asset were found after that.

After the incident, as an immediate response, the local government approved funds to shore up the other sections of the viaduct, following an emergency protocol involving structural stabilization, traffic interruption, and detours. In parallel, a trilateral partnership between the Department of Roads and Highways (DER), the public engineering company NOVACAP, and the Structural Department of the University of Brasilia (UnB) was assembled. Their goal was to investigate the partial collapse, develop a retrofitting plan for the asset, and assess other specific viaducts and bridges built during the same period. This mobilized over $32 million in investments for assessing, monitoring, and strengthening specific infrastructure, including the retrofitting of 96 cloverleaf passages, the strengthening of 40 strategic viaducts, and the construction of four additional highway bridges, according to the Brasilia Local Agency (2019) [3].

There are a few documented reports of similar collapses, such as the failure of the Wilkins Air Force Depot in Ohio in 1955 [4–6]; however, those involving special heritage structures made with prestressed concrete are even scarcer. Recently, two documented studies of bridge collapses have been published (the Morandi Bridge failure in 2018 and the FIU pedestrian bridge failure, also in 2018) [7,8]. Although these bridges do not possess geometric similarities to the viaduct investigated in the present manuscript, they also represent sudden collapses related to either tendon mechanical deterioration or overloads/deficient design, respectively. Given this scenario, this paper presents distinct engineering characteristics and failure mechanics of the South Road Axis Viaduct that remain insufficiently examined. This case study presents unique features and challenges of the intervention, gathered in a detailed forensic investigation.

2. Methodology

Overall, the authors' methodology consisted of an in-depth forensic investigation, followed by manual and numerical calculations of the viaduct.

In detail, the forensic investigation comprised an extensive collection of data from the existing structure: searching for and gathering available construction documentation, in situ debris investigation, core sample extraction and examination, and geometrical and mechanical characterization. It is important to mention that many original documents for monuments in Brasilia could not be retrieved from public archives due to their age and inappropriate storage protocols at the time of construction, including those for the current viaduct, thereby imposing a challenging research constraint. Nonetheless, the collection of the asset's data allowed a transparent representation of the existing structure. During this step, intrinsic issues related to the construction of the South Road Axis Viaduct became evident. Details of these problems are thoroughly highlighted in this manuscript.

Furthermore, design verifications for the ultimate limit state were performed in accordance with modern Brazilian standards [9–11] and compared with finite-element numerical modeling using ABAQUS software [12]. This enabled a comprehensive diagnosis of the viaduct based on RC failure mechanics. Lastly, a description of the retrofitting and repair techniques employed in the viaduct's recovery is presented.

Disclosure: The first and fourth authors of this study participated in the trilateral partnership that conducted investigations of the viaduct. The first author was a member of the University of Brasilia engineering department, while the fourth author is an employee of the NOVACAP structural engineering department.

3. Forensic Investigation

The forensic investigation comprised a thorough collection of data from the existing structure: available construction documentation (including technical drawings, project information, and intervention records), in situ debris investigation (including the demolition of specific segments of the viaduct and concrete members), invasive testing (core extractions from concrete members and reinforcing steel amputations), geometrical characterization (in situ measurements), and mechanical characterization (rupture tests of collected samples conducted at the University of Brasilia). Since many original documents from the viaduct were missing or unavailable in public archives, in situ exploration was deemed necessary. For this reason, geometric characterization, as well as the demolition of specific structural components, was imperative for understanding the asset's structural geometry and engineering characteristics.

3.1. Viaduct Engineering Anatomy

The construction of the viaduct at Galeria dos Estados took about 3 months between 1959 and 1960 due to political pressure for the city's grand opening [13]. The shape of the main structure was envisioned by Oscar Niemeyer and designed by engineer Bruno Contarini. An overview of the main structural components of the viaduct is shown in Figure 2:

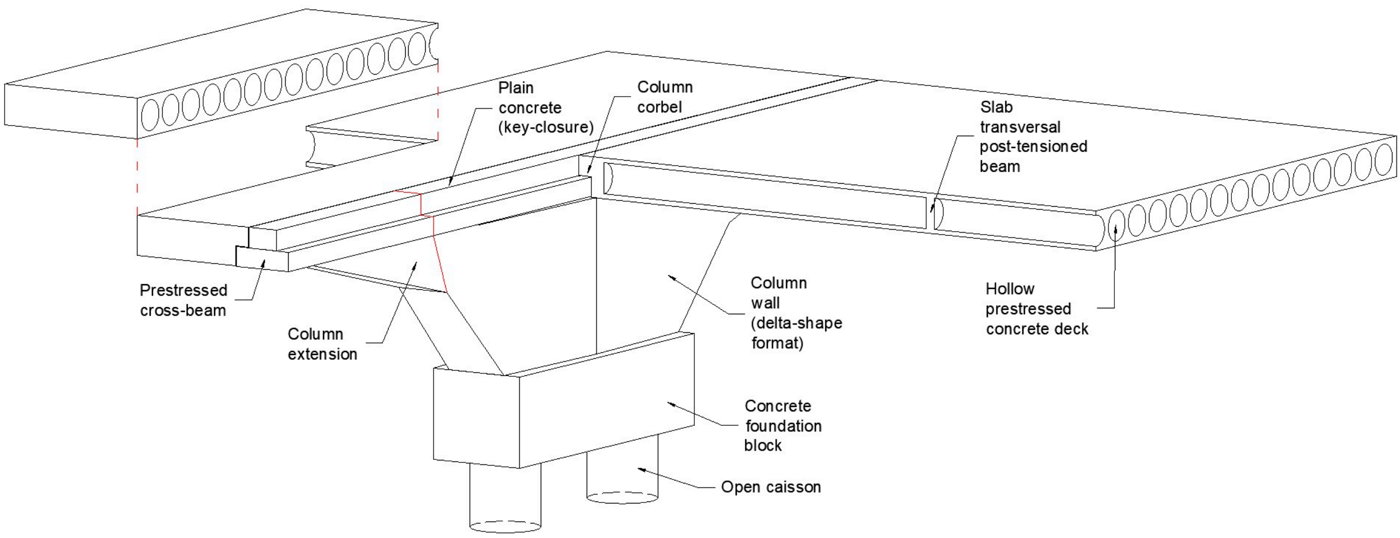

Figure 2. Three-dimensional view of the viaduct's structural components, with indication of failure plane and slab projection.

The asset structure comprises seven large column walls with a unique delta-wing shape and 7.4 m cantilevered extensions, reaching approximately 28 m in full width. The column wall thickness varies from 96 cm (at its extension edge) to 200 cm (at its center)—a common design feature observed in many monuments across the capital (varying cross-sections). The reinforcing steel of this element comprised smooth bars, as shown in Figure 3 (left side, in magenta). Cross-section drawings of the critical section are shown in Figure 4.

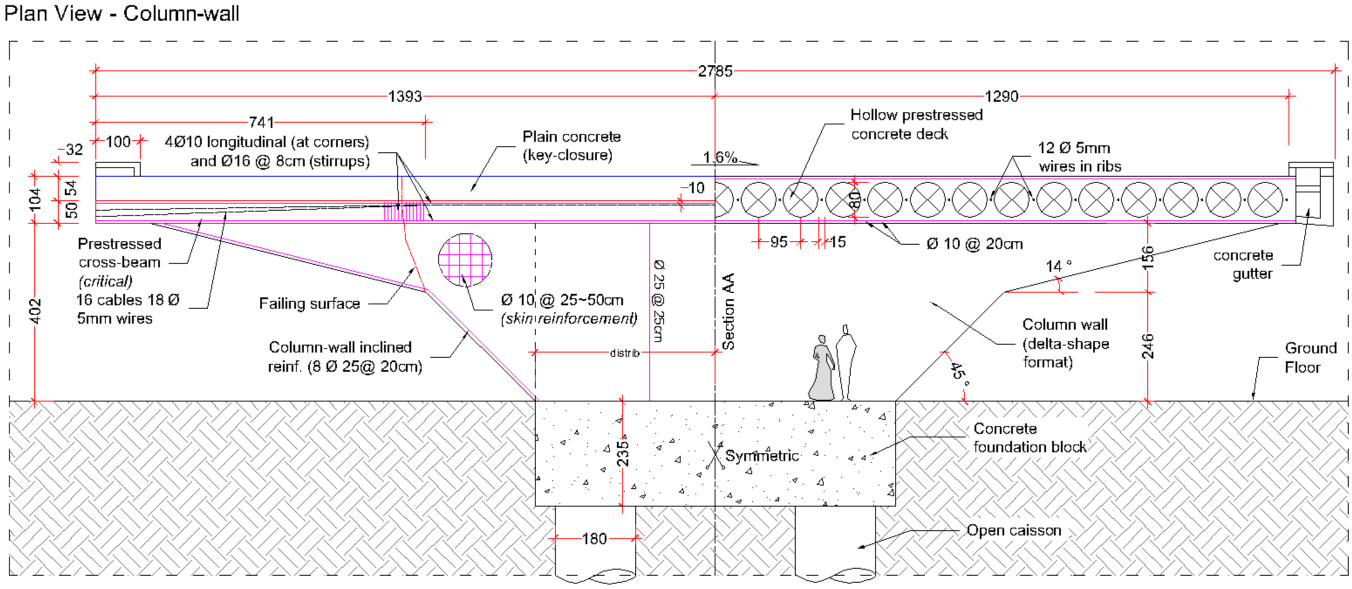

Figure 3. Plan view of the column wall in cm. Left: details retrieved through site investigations (indicating reinforcing steel in magenta and plain concrete in blue). Right: hollow prestressed concrete deck; units are in cm (with dimension lines in red). ø = diameter of rebars; @ = spacing of centers.

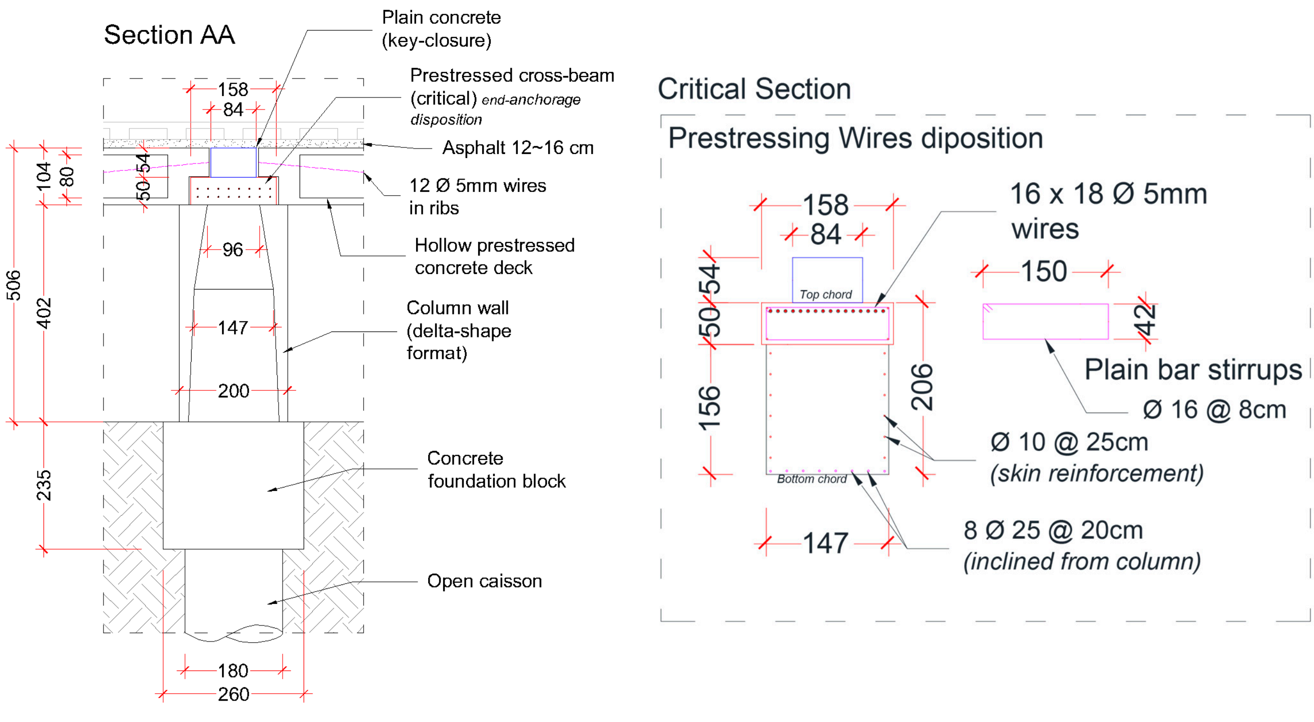

(**a**) (**b**)

Figure 4. Detailing retrieved from site investigations: (**a**) Section AA of the column wall, which supports the hollow deck; (**b**) critical section for computing the capacity of the element. Units in cm, rebars are in magenta, plain concrete is in blue, dimension lines in red, ø = diameter of rebars; @ = spacing of centers.

The column walls meet eight simply supported prestressed hollow concrete core slabs, which form a seven-lane vehicle deck, resulting in a total viaduct length of 194 m. Two abutments at the viaduct's free ends connect the asset to the Road Axis. The deck is slightly tilted (about 1.6% inclination) along the main road, following a small street curvature, which also helps with water drainage since the city experiences heavy seasonal rains. This marginally changes the geometry of each column wall, as shown in Figure 3.

The hollow core slab is 104 cm deep, and its span is about 22 m between column supports. The edges of the slabs are solid concrete, supported by bearing pads over the column corbels (see Figures 2 and 4a). At the center of the deck, there is one prestressed transverse beam (see Figure 2) connecting the 80 cm-diameter hollow cores to reduce dead weight. These cores are spaced 95 cm on center, creating 15 cm prestressing ribs within the deck to increase shear and flexural strength. Besides the longitudinal prestressing cables, the hollow slabs had reinforcement in the transverse and longitudinal directions (10 mm-diameter smooth bars, spaced 20 cm on center).

Another important detail of the assembly is the inverted T-beam extension of the column wall. It is, in fact, composed of two rectangular elements attached to one another where the failure occurred (see Figure 4a). The lower section (red rectangle 158 $\times$ 50 cm^2) is a prestressed concrete cross-beam comprising 16 strands (18 wires, 5 mm diameter each), while the upper section (blue rectangle 84 $\times$ 54 cm^2) is a key-closure plain concrete encasement. This key insertion of plain concrete was poured after the placement of the concrete slabs to seal off the prestressing cables from moisture, which was intended to isolate and protect the anchorage systems of these members. Therefore, this unreinforced element was not fully attached to the main cross-beam, nor could it attain flexural or shear resistance due to the lack of reinforcing steel. Thus, this element should be ignored in design calculations.

Furthermore, the prestressed cross-beam was designed with a small amount of conventional longitudinal reinforcing steel (smooth bars, 10 mm diameter at stirrup corners), a limited number of single stirrups (smooth bars, 16 mm diameter, 8 cm on center), and 16 prestressing strands (post-tensioning cables, possibly with BBRV anchorage for buttonhead wedge system, or similar). There were no stirrups below the prestressed cross-beam, only small amounts of longitudinal skin reinforcement distributed through its depth (as per Figure 4b). Also, there were 8 face bars (bent and inclined, as per Figure 3), consisting of 25 mm-diameter bars that followed the shape of the column wall. These bars improved the dowel action at the element's extension.

Regarding the amount of steel in the critical section, steel areas were verified for both longitudinal (passive and active) and transverse reinforcement. The critical section had a passive reinforcing steel ratio of less than 0.16% and a prestressing steel ratio of 0.18%. These values are fairly analogous to the minimum 0.15% required by the modern Brazilian standard, usually adopted to prevent cracks caused by concrete shrinkage. On the other hand, the transverse reinforcement ratio was 0.32%, considering a minimum transverse reinforcement ratio of 0.16% for linear elements with concrete strengths below 30 MPa. These values tend to differ for volumetric elements (such as corbels and foundation blocks) compared to linear elements.

The post-tensioning system employed in the viaduct consisted of galvanized metal ducts through which grout was pumped to protect the steel wires embedded within the strands. This technique is still employed today, as it is a safe method for preventing stress corrosion of wires (which is critical in prestressed concrete structures) and for bonding the wires to the surrounding concrete.

The original design drawings of the viaduct structure were missing from public and administrative archives; however, NOVACAP had geometrical representations of the viaduct developed in 2013. These as-built drawings, along with information collected during the dismantling of some sections, helped the forensic team develop the images for this manuscript.

https://doi.org/10.3390/buildings16193806

3.2. Materials Characterization

After the incident, samples were extracted from target sections (four concrete cores were retrieved, two from each column wall) and tested at the University of Brasilia's laboratory for mechanical characterization. Samples of post-tensioning wires (14 samples) and passive reinforcing steel rebars (10 samples) were extracted and assessed at the same lab. Some concrete sections were tested with the phenolphthalein indicator to evaluate carbonation depth.

Lab results indicated that the nominal concrete strength was surprisingly high (43.8 MPa and 43.3 MPa for column wall 7 and 33.37 MPa and 27.9 MPa for column wall 6). Also, these values indicated high variability within the sections, suggesting some stratification of concrete strengths throughout the element's volume. Since the cross-beam was damaged, core samples were extracted from the columns. Additional core samples should have been extracted due to the high variability; however, limited resources and time constraints prevented further exploration.

Also, the steel wire strengths varied from 1100 MPa to 1400 MPa, while those of regular passive steel varied from 200 MPa to 350 MPa. Young's modulus was determined to be about 205 GPa. Steel rebars were extracted from various locations in the elements. Carbonation tests indicated that carbon dioxide reached depths beyond the nominal concrete cover in some regions, suggesting that reinforcing steel may have been subjected to corrosion. This was confirmed during tension tests of steel rebars, where some bars suffered severe loss of nominal area due to corrosion (some samples lost up to 50% of their original transverse area) [13]. However, the overall quality of the concrete material was considered adequate for a possible repair or retrofitting of the asset. Concrete core and steel sample extractions followed strict protocols from Brazilian standards NBR 7680:2015 (for concrete) [14] and NBR 6349:2008 [15], NBR 6892:2002 [16], and ISO 15630-1:2010 (for steel alloys) [17].

At the time of construction, normal concrete compressive strength ranged from 20 to 25 MPa, and regular steel alloys were typically CA-32 (fyk = 320 MPa), while prestressing steel wires had normal relaxation. Detailed information on the results from material characterization can be found in [13,18,19].

It should be noted that there are limited data from concrete characterization, as only two specimens were extracted from each column wall at the time of the incident. Since this is the only available public information gathered, the authors used it with caution, as further addressed in Section 3.5.

3.3. Failure Chronology and Debris Investigation

According to site investigations and camera recordings from monitoring devices along the South Road Axis, the collapse occurred around midday, when a large section of the deck suddenly collapsed (see Figure 5). There were no warning signs, such as large deflections or settlements, revealing that the failure was brittle and resulted in partial collapse.

Local assessment of the debris and site scene revealed that the failure mechanism started with the shear failure of column wall P7 (indicated by the smooth "clear" section in Figures 6 and 7b) at the beginning of the extension of the element, where there is a transition from the delta shape to the column cantilever extension.

https://doi.org/10.3390/buildings16193806

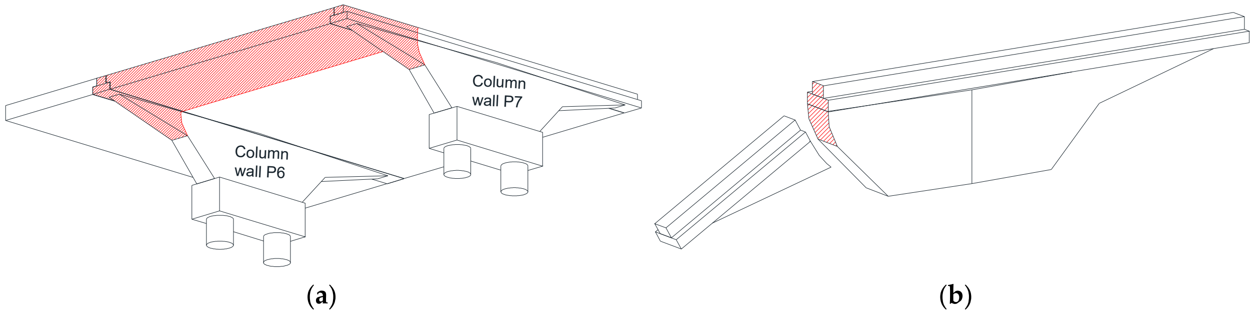

Figure 5. (**a**) View of the deck section that collapsed (in red); (**b**) indication of the plane of failure of column wall P7 at the beginning of the cantilever extension (in red).

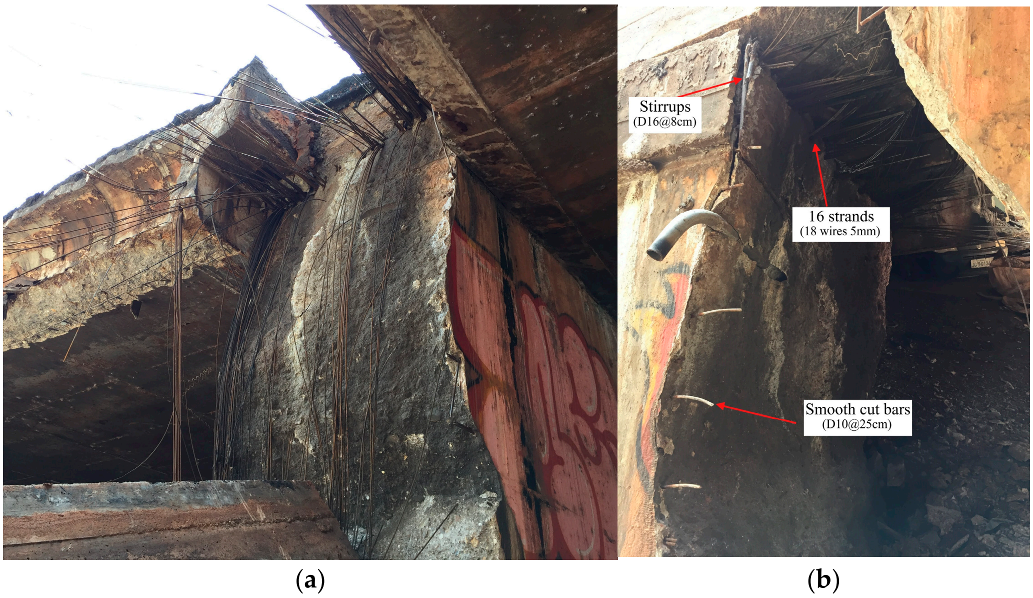

Figure 6. Investigation of the debris: (**a**) close-up view of column wall P7, indicating the smooth section, cut strands, and water infiltration; (**b**) fallen column-wall extension after collapse, indicating the small-diameter smooth bars and the stirrups only at the top of the prestressed cross-beam.

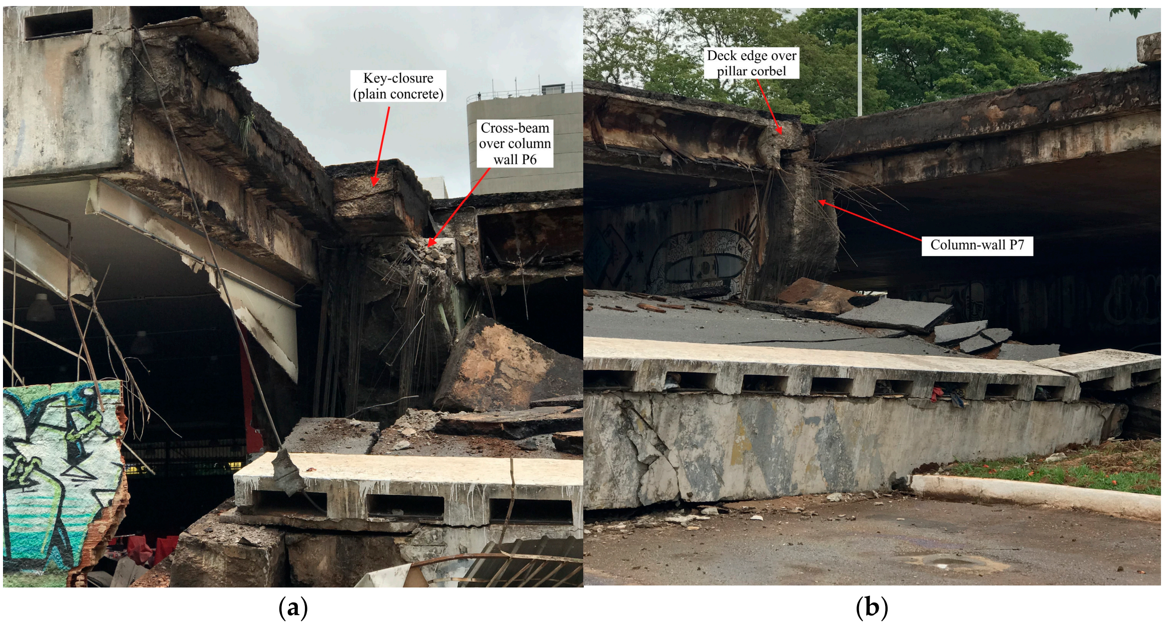

Figure 7. Investigation of the debris: (**a**) column wall P6 fracture; (**b**) column wall P7 fracture.

Once the column-wall extension at P7 collapsed, the right support of the concrete hollow deck began to move downward due to the loss of equilibrium. This movement pulled the other end of the deck, which was connected to the top of column wall P6 by the plain concrete key closure and the deck prestressing anchorage. The movement of this massive section generated immense kinetic energy, which was partially absorbed by the cross-beam of column wall P6 (which presented the same chronic deficiency as column wall P7). This created a large, unbalanced lateral force that exhausted the remaining capacity of the cross-beam at column wall P6, fracturing it by pullout and shear, spalling the concrete, and damaging adjacent members (as seen in the destroyed surface in Figure 7a). The last component of the concrete hollow deck was its prestressed transverse beam, which was unable to support all the remaining loads from the system. This last element also failed under shear, creating a smooth surface evident on site, as shown in Figure 8a (highlighted by the center arrow). Additionally, a large longitudinal crack was present across the road lane in all deck sections adjacent to the partially collapsed deck, indicating that endemic problems were not exclusive to this region. This crack is shown in Figure 8b.

(**a**) (**b**)

Figure 8. Investigation of the debris: (**a**) section of the deck that collapsed, highlighting the transverse beam that failed under shear (indicated by the red arrow); (**b**) large longitudinal asphalt crack across the deck next to the fallen section between column walls P5 and P6.

The significant variability in concrete compressive strength observed between column walls P7 (43.8 MPa) and P6 (33.37 MPa) highlights the inherent spatial heterogeneity of the pillars. However, the initiation of failure at P7—despite its higher sampled compressive strength—strongly indicates that concrete compressive capacity was not the governing factor in the collapse sequence. Instead, the failure suggests the dominance of geometric discontinuities and inadequate reinforcement detailing/mechanical degradation. This is discussed in Section 4.

Additionally, engineering teams were unable to assess the structure across the viaduct because a restaurant had been located underneath the viaduct, where infill partition walls and ducts obstructed the view of the pillars. Once these elements were removed or demolished, engineers were able to detect several problems, including severe cracking and chronic water infiltration, in all column walls. These problems are indicated in Figure 9.

(**a**) (**b**)

Figure 9. Investigation of the debris: (**a**) column wall P7 (on the end that did not collapse), indicating the propagation of the inclined crack and water infiltration (which was common to all columns); (**b**) underside view of the prismatic key-closure element over the fallen column-wall extension P6, where signs of chronic water infiltration were detected (in the locations pointed by the red arrows).

Engineers were also able to evaluate the quality of the materials employed during the construction of the viaduct. They detected a lack of cementitious mortar (grout) in several strands of prestressing cables, as per Figure 10a. Additionally, the concrete was composed of rounded river gravel aggregate rather than conventional limestone coarse aggregate. This evidence can be seen in Figure 10b.

(**a**) (**b**)

Figure 10. Investigation of the debris: (**a**) concrete made with rounded river gravel aggregate and absence of grout in strands (indicated by arrows); (**b**) absence of grout mortar within the prestressing strands and stress-corroded steel wires.

In addition, degradation at the base of the column wall was identified by extensive corrosion of the column rebars, along with concrete spalling and cracking of the nominal cover, as seen in Figure 11a. This region is usually targeted by homeless people, with unsanitary conditions exposing the concrete to aggressive chemical agents. Lastly, at the base of the column wall, inclined bars from the extension faces had peeled out during the collapse of the extension as they resisted the partial collapse through dowel action. This is shown in Figure 11b.

(**a**) (**b**)

Figure 11. Investigation of debris: (**a**) severe corrosion of column rebars near ground level; (**b**) fallen section, indicating cut rebars and inclined column bars that had peeled out.

3.4. Standard Recommendations in 1960—A Historical Overview

The first published standard on the design of prestressed structures in Brazil was NBR 7197 (Design of Structures made with Prestressed Concrete) [20], published in 1989. Before this period, engineers followed the guidance of NB1 (Design of Concrete Structures) [21] and NB2 (Design and Construction of Bridges) [22]. However, NB1 was first published in 1940 and then updated in 1953 and 1960, while NB2 was first published in 1941 and then updated in 1961. For the determination of actions on bridges, designers followed the recommendations in NB6 (Vehicle Loads on Highway Bridges) [23], which was first published in 1960.

Chronologically, given the construction period of the South Road Axis Viaduct (between 1959 and 1960), engineers had to follow other design guidelines set out in international standards. In other words, Brazilian national standards were either absent or lacked sufficient information on the behavior of large prestressed concrete bridges.

Among the available standards at the time, engineering faculties employed some pioneering and traditional literature, which was mainly based on [24]:

- ACI 318-51 (Building Code Requirements for Reinforced Concrete, 1951);
- AASHO/49 (Standard Specification for Highway Bridges, 1949);
- GB/48 (British Standard Code of Practice for Structural Use of Normal Reinforced Concrete in Buildings, 1948);
- DIN 1072 ("Straßen- und Wegbrücken—Lastannahmen"—Loads on Road and Pedestrian Bridges, 1950);
- DIN-1045 ("Beton—und Stahlbetonbau—Bemessung und Ausführung"—Design and Construction of Concrete and Reinforced Concrete Structures, 1952);
- DIN 4227 ("Spannbeton—Richtlinien für Bemessung und Ausführung"—Design of Prestressed Concrete Structures, 1953).

Many of these standards served as fundamental instructions for the development of recognized European codes, like the CEB/fib series after the 1970s.

Regarding the available Brazilian specifications at the time (NB1 and NB2), shear design was based on principal stresses and checked for the required transverse reinforcement. Most of the previous international codes checked shear design by limiting shear stresses in concrete elements (for example, 0.4—0.6 MPa for beams without transverse reinforcement, and 1.4–2.0 MPa for beams with transverse reinforcement)—values agreed upon limited experimental campaigns, and insufficient modeling options at the time.

In the case of NB1 and NB2, maximum shear stresses were limited $1.3f_{cm}/25 \leq$ 0.8 MPa for elements without transverse reinforcement, and $1.3f_{cm}/10 \leq 2.0$ MPa for elements with transverse reinforcement. The Brazilian standards recommended checking this requirement for combined shear and torsional moments for the ultimate limit state (ULS) for prismatic elements. When minimum amounts of shear reinforcement were employed, minimum spacing requirements (such as d/20) could be adopted. Also, it was common practice to use part of the bottom beam longitudinal reinforcement, bent up and anchored at the member's end, as top reinforcement. This bent bar was considered in shear design by assuming it contributed to carrying part of the shear stress from the stirrups.

For prestressed elements, Brazilian engineers determined the required stirrup spacing based on the amount of tension the stirrups would absorb, given the presence of prestress (if prestress was not considered, the stress would be entirely absorbed by the stirrups). The level of stress was determined from the principal stresses in mechanics [25]. At that time, it was believed that shear failure would be less critical in design since flexural failure would govern the ULS. In addition, shear design had not yet evolved to the generalized truss analogy from Mörsch's method, at a time when laboratory experiments were scarce. Therefore, important phenomena and parameters that usually impact the shear behavior of concrete elements (such as size effect, progressive collapse, fatigue, and cyclic deterioration) were not fully explored or documented in Brazilian codes at that time.

Conversely, the design of longitudinal reinforcement, whether non-prestressing or prestressing steel, employed either the Rupture Method (equivalent to ULS) or the Allowable Stress Design (ASD). The older version of NB1 allowed tension reinforcement to consist of bars or wires, but no minimum amount of non-prestressing steel was specified to avoid progressive collapse. The minimum amount of tension reinforcement varied from 0.15% to 0.2% based solely on the steel strength class. Hence, engineers had insufficient technical guidance during the construction of the South Road Axis Viaduct compared with today's requirements for quality control and management.

Furthermore, the former NB6 specified a moving load type called "TB36" (vehicle weight of 360 kN), distributed among three-wheel axles (6 m $\times$ 3 m). Moving loads were increased by a factor of approximately 1.25 to account for the vertical impact. Additional traffic loads were applied in the primary (5 kN/m^2) and secondary (3 kN/m^2) lanes. Nowadays, traffic demands have increased considerably compared to the previous requirements of NB6: the maximum vehicle load is determined by TB450 (450 kN vehicle weight), the lane traffic load is about 5 kN/m^2, the additional asphalt weight from repairs is 2 kN/m^2, and two additional coefficients increase the vertical load impact (number of lanes coefficient (CNF) and additional coefficient of impact (CIA)) [9]. Accordingly, estimates of new load demands can increase by up to 22.5% compared to the older requirements.

3.5. Demands and Theoretical Strengths

To determine the section's resistances, the authors used the recommendations of the Brazilian standard (NBR 6118:2025) [11], whose formulations are similar to those of Eurocode 2 [26] for flexural design. In terms of shear design, although there are some conceptual similarities, the NBR model is broader, allowing the designer to freely select the model (either I or II) and the inclination of the compressive strut. The shear models in the Brazilian standard essentially differ in their consideration of shear absorbed by the concrete mechanism, which the designer arbitrarily selects. Eurocode 2 tends to be slightly more conservative than NBR 6118.

It is important to highlight that all manual calculations (and later numerical inputs) used the nominal values of the materials ($\gamma_c = \gamma_s = 1.0$), as well as unfactored loads ($\psi = \phi = 1.0$). As per the materials characterization in Section 3.2, the authors chose the following upper-bound material values, specifically related to column wall P7 (the element that triggered the collapse): fc = 43.8 MPa, fyp = 1400 MPa, fy = 350 MPa, and

Es = 205 GPa. The upper-bound material strengths would imply the best performance of the structure—this is the scenario evaluated and discussed throughout this manuscript.

Since the critical section is under-reinforced through its depth (only the cross-beam has both stirrups and longitudinal reinforcement), the definition of effective depth might be debatable. Also, size effects play an important role in reducing the shear strength of RC elements without transverse reinforcement [27]. These factors might invalidate the truss analogy formulation used to determine the shear strength for the whole section; thus, only the cross-beam section should be considered in the capacity analysis. For this reason, the use of numerical simulation is strongly recommended for this assessment.

The authors estimated unfactored bending moments (Mn) and shear forces (Vn) at the critical section, considering dead loads from the section's elements and the live load from the standard-weight vehicle (TB36 tf). The most unfavorable position of the vehicle was at the edge of the cross-beam, where the traffic loads per lane matched this arrangement. Alleviating prestressing forces were also estimated based on the information collected. A summary of these loads is presented in Table 1.

Table 1. Share and nature of internal loads across the viaduct's critical section.

Nature of Loading	Mn (kNm)	%	Vn (kN)	%
Dead	6195.3	59.8%	1853.5	64.2%
Vehicles with TB36	4171.2	40.2%	1034.3	35.8%
Total	**10,366.5**	**100.0%**	**2887.8**	**100.0%**
Prestressing	−4875.5	78.7% [1]	−658.0	35.5%

[1] Percentage considering the balancing of the dead load only.

As shown in Table 1, the total bending moment demand over the critical section is 10,366.5 kNm, while the total shear demand is around 2888 kN. For the critical section shown in Figure 4b, the resisting bending moment (considering section equilibrium) is about 11,980.4 kNm, corresponding to a capacity demand of 86.5%. The flexural strength of the section was determined using nominal strengths (no reduction factors applied to the material strengths) for a total of 16 cables.

Had there been 13 cables (assuming that 3 cables had been lost due to stress corrosion, a 19% steel reduction), the nominal flexural strength would be 9809.1 kNm, representing over 105% of the capacity. Conversely, if contemporary vehicle loads had been assumed (for example, the use of TB450 in the calculation), flexural demands could have increased to 12,092.5 kNm, exceeding the available capacity of the member. This suggests that if very few cables had had problems or if load demands had been higher than previously estimated, the flexural capacity of the column-wall extension could have been critically jeopardized.

In terms of shear strength, the determination of the section shear capacity can be complicated since stirrups did not extend through the whole critical section depth, considering the generalized truss theory. As indicated in Figure 4b, transverse reinforcement is present only in the prestressing cross-beam, which has an effective depth of 37 cm. If the entire cross-section is considered, the effective depth is 193 cm, which is much larger than the former. This, however, should be carefully considered since the lack of transverse reinforcement could violate the hypothesis of the generalized truss model or jeopardize the strut anchorage and tie action within the section. Perhaps a more sophisticated method of calculation could be employed, such as the strut-and-tie method (STM), to assess the strength. Either way, the authors determined the shear strength for both effective depths using models I and II with varying strut inclinations. The results are presented in Tables 2 and 3. The effective depth of 37 cm represents the screening lower bound, while the effective depth of 193 cm represents the upper bound of shear strength, according to the generalized truss model.

Table 2. Hypothetical shear strength of the critical section, considering an effective depth of 37 cm (screening lower bound of shear strength), assuming the generalized truss model.

deff = 37 cm	**Model I**		**Model II (θ = 45°)**		**Model II (θ = 30°)**	
Prestress	without	with	without	with	without	with
Vs (kN)	2887.8	2295.6 [1]	2887.8	2295.6 [1]	2887.8	2295.6 [1]
VR2 (kN)	5702.2	5702.2	5702.2	5702.2	4938.3	4938.3
VS/VR2 (%)	50.6%	40.3%	50.6%	40.3%	58.5%	46.5%
Vc (kN)	653.7	1045.4	364.5	705.4	312.9	644.8
Vsw (kN)	585.8	585.8	585.8	585.8	1014.7	1014.7
VR3 (kN)	1239.5	1631.2	950.3	1291.2	1327.6	1659.5
VS/VR3 (%)	**233.0%**	**140.7%**	**303.9%**	**177.8%**	**217.5%**	**138.3%**

[1] Alleviating effects of prestress considered 90% of the total prestressing force balancing Vs, as a standard engineering practice in Brazil ($2295 \approx 2887 - 0.9 \times 658$).

Table 3. Hypothetical shear strength of the critical section, considering an effective depth of 193 cm (upper bound of shear strength), assuming the generalized truss model.

deff = 193 cm	**Model I**		**Model II (θ = 45°)**		**Model II (θ = 30°)**	
Prestress	without	with	without	with	without	with
Vs (kN)	2887.8	2295.6 [1]	2887.8	2295.6 [1]	2887.8	2295.6 [1]
VR2 (kN)	29,744.1	29,744.1	29,744.1	29,744.1	25,759.1	25,759.1
VS/VR2 (%)	9.7%	7.7%	9.7%	7.7%	11.2%	8.9%
Vc (kN)	3410.2	5453.1	3477.8	5683.8	3489.8	5725.0
Vsw (kN)	3055.9	3055.9	3055.9	3055.8	5292.9	5292.9
VR3 (kN)	6466.1	8509.0	6533.7	8739.6	8782.7	11,017.9
VS/VR3 (%)	**44.7%**	**27.0%**	**44.2%**	**26.3%**	**32.9%**	**20.8%**

[1] Alleviating effects of prestress considered 90% of the total prestressing force balancing Vs, as a standard engineering practice in Brazil ($2295 \approx 2887 - 0.9 \times 658$).

In the tables, Vs is the shear (unfactored) demand, VR2 is the (nominal) strength of the concrete compressive strut, Vc is the concrete (and mechanisms) shear (nominal) strength, Vsw is the shear (nominal) strength of the stirrups, and VR3 = Vc + Vsw is the total section shear (nominal) strength.

As can be seen, the shear capacity of the critical section, with an effective depth of 37 cm, is insufficient to meet the load demand, as the capacity index (VS/VR3) exceeds 100%. This occurred for all shear models and strut inclinations, with the demand exceeding the theoretical shear capacity by an average of 202%. Yet, when the section's effective depth is 193 cm (even though the truss formulation might be invalid), the shear capacity is adequate, independent of the model, strut inclination, and the alleviating effects of prestressing forces. In this scenario, the average shear capacity is about 32.6%. It is possible that the effective shear strength of the viaduct falls somewhere in between or even closer to the cross-beam (deff = 37 cm) strength. If the shear demand is determined based on the resisting moment strength (MR), the shear demand to reach the full theoretical beam strength is 3233.6 kN. This is addressed in Section 3.6 of this work.

Regarding section stresses—a required step in determining the performance of prestressed concrete elements—the critical section was evaluated under three load combinations commonly employed by the Brazilian standard. Service load combinations included the quasi-permanent combination (CQPerm), the frequent combination (CFreq), and the rare combination (CRare). Their quantification accounted for the influence of prestressing forces, assuming 30% total losses based on the prestressing system and material characterization. This value of prestressing loss was selected based on standard engineering practice for post-tensioning systems and includes immediate and time-dependent losses, plus some possible loss of strength due to environmental degradation. Stresses were determined for the actual section, which contained 16 cables, and for a section containing 13 cables for comparison. The results are presented in Table 4.

Table 4. Determination of nominal stresses (manually calculated) for the critical section.

Stress in Critical Section (MPa) *			
Location/Load Comb	**CQperm**	**CFreq**	**Crare**
Top chord (16 cables)	1.60	1.96	3.07
Bottom chord (16 cables)	−5.19	−5.56	−6.67
Top chord (13 cables)	2.76	3.13	4.25
Bottom chord (13 cables)	−5.68	−6.05	−7.17

* Negative values are in compression; positive values are in tension.

Table 4 shows that the critical section was operating under tension for service load combinations, suggesting that the prestressing system was partial. According to Brazilian standard NBR 6118, the concrete stress limits were determined for tension (3.94 MPa) and compression (−26.31 MPa) under service conditions.

In conclusion, even though stresses were below the concrete tension limit considering 16 cables, the column-wall extension was prone to developing tension cracks at the critical section, as tension would control independently of the load combination. Had the effective number of cables been reduced (to 13, for example), the concrete tension limit would have been exceeded for the rare combination, and cracks could have developed.

Finally, the authors also quantified the dowel strength of the passive reinforcing steel based on the Rasmussen BH model [28]. This model was experimentally validated and quantifies the individual shear strengths of rebars and bolts for both smooth and deformed metal bars. The dowel action, considering all the passive longitudinal steel in the critical section, was estimated to be 998 kN by this model, carrying less than 35% of the estimated shear demand. In other words, had a shear hinge developed within the critical section after the initiation of a plane of failure, the dowel action would have been insufficient to prevent partial collapse. Evidence of this hypothesis is shown in Figure 11 by the peeling out of the inclined column bars. Additionally, the dowel strength was determined using the A.H. Mattock and N.M. Hawkins model [29] and the E.N. Vintzeleou and T.P. Tassios model [30], and the results are presented in Table 5.

Table 5. Dowel strength according to different models in the literature.

Model	Year	Dowel Strength (kN)	Vs/Vdowel (%)
Rasmussen BH	1963	998.0	289.4%
Mattock AH and Hawkins NM	1972	681.7	423.6%
Vintzeleou EN and Tassios TP	1986	1151.5	250.8%

As can be seen in Table 5, the range of dowel strengths (Vdowel) from these different models would indicate insufficient safety after the slip of the critical section. The estimation of the passive reinforcement's dowel action capacity using the E.N. Vintzeleou and T.P. Tassios model serves as a theoretical upper-bound baseline for evaluating shear transfer. Their formulation includes cyclic deterioration and cracking of the section, providing a consistent model on which to base this analysis. When accounting for large-diameter rebars and a large cracked volume of the section, bond behavior could further compromise the concrete wedge resistance upon which the dowel mechanism relies. This could affect the idealized model and overestimate the actual shear contribution of the passive bars. In the end, this limitation further supports the structural deficits identified in the forensic analysis: the true dowel action capacity could have been even lower than that estimated by the models, revealing a deficiency in the internal shear-transfer mechanisms that would have reduced structural redundancy against progressive collapse.

3.6. Numerical Evaluation

3.6.1. Boundary Conditions and Materials

Due to the limitations of manually calculating the strength of complex elements, specifically in determining the effective depth and stresses in the column-wall extension, numerical simulations were performed. For this purpose, an ABAQUS/CAE model was developed to assess the structural response and failure mechanisms.

For simplicity, half of the column wall was modeled across its symmetry axis using 3D solid elements for concrete (column core and cross-beam extension) and wire (truss) elements for reinforcing bars (both passive steel and prestressing strands). The units employed were N and mm. A view of the model and its reinforcement is shown in Figures 12a and 12b, respectively.

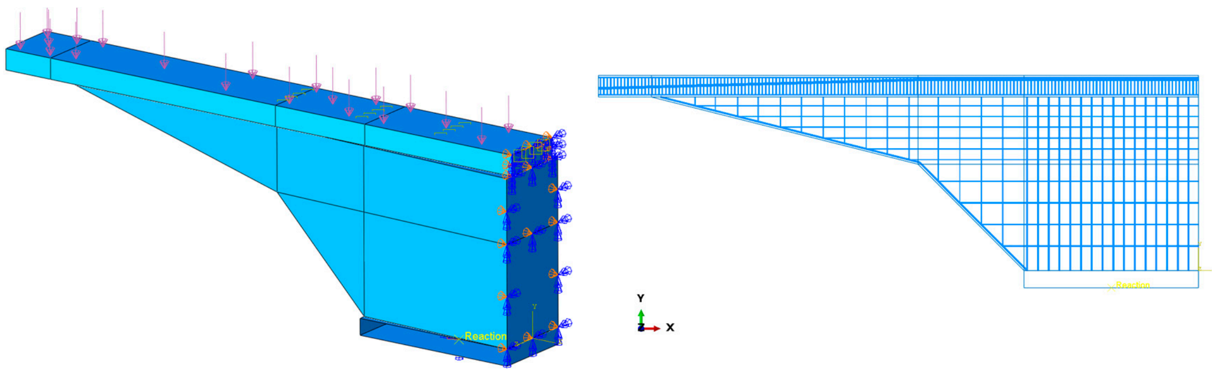

(**a**) (**b**)

Figure 12. ABAQUS model of half of a column wall: (**a**) geometry and boundary conditions; (**b**) steel cage arrangement.

The column wall was supported by an analytical base (rigid element) tied to a reaction node to simulate a fixed support condition. In addition, the boundary condition at the end surface (center of the wall) prevented sidesway (simulating the other column half) by imposing zero horizontal displacement—a standard procedure to improve numerical simulation efficiency. Three-dimensional concrete finite elements were modeled using eight-node linear elements with reduced integration and hourglass control, while steel bars and wires were modeled using two-node linear 3D trusses. Steel was perfectly embedded in concrete—an interaction property commonly employed in ABAQUS that prevents bond slip of rebars. Since the sections were large (over 12 m in length), the finite-element mesh employed was 25 cm × 25 cm, as shown in Figure 13a.

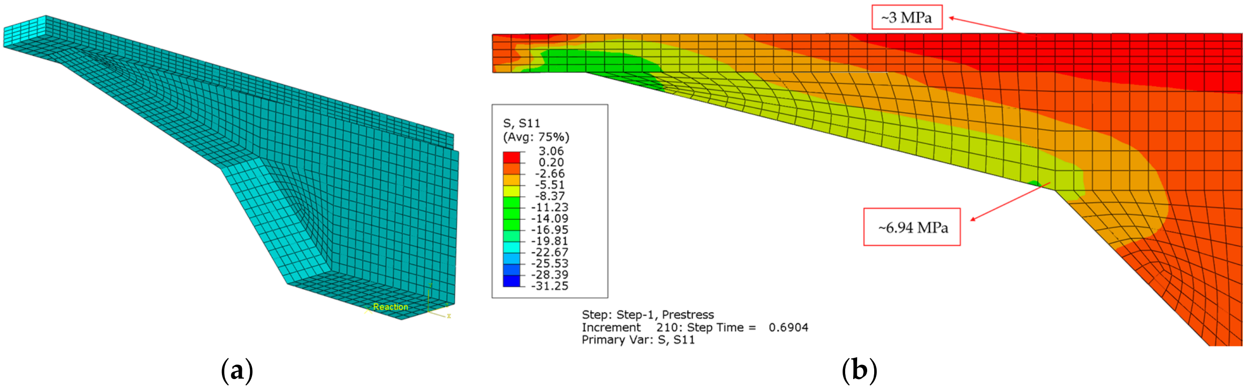

Figure 13. (**a**) Finite-element mesh arrangement; (**b**) level of stress for estimated service demands, showing that the top chord was operating under tension.

Self-weight loads were automatically calculated by the software based on section geometries and material densities. At the same time, prestressing forces were induced by predefined fields, and service loads were imposed as surface pressures over the cross-beam. Figure 13b shows the level of stress in the critical section under operational loads, which is fairly similar to that manually calculated and displayed in Table 4 for Crare.

Concrete material was modeled according to the ABAQUS built-in concrete damage plasticity (CDP) model, which considers two primary failure mechanisms (tensile cracking and compressive crushing). This model allows users to quantify concrete damage using a damage index determined from concrete stress–strain curves. The compressive concrete curve was based on the model of Mander et al. [31], which disregarded the effect of uniaxial confinement provided by transverse reinforcement. The nominal concrete compressive strength from column wall P7 was adopted (43.8 MPa). On the other hand, the tensile concrete curve was based on the Cornelissen–Hordijk–Reinhardt tension-softening curve [32].

These selected concrete models usually converge efficiently with the ABAQUS CDP model. Generally, for the mechanical representation of steel, reinforcement follows a bilinear stress–strain curve with strain hardening for both passive and active steel. This model effectively characterizes the mechanical behavior of steel under monotonic loading. Figure 14 shows the stress–strain curves for concrete (under compression and tension) and steel, used as inputs within the ABAQUS interface.

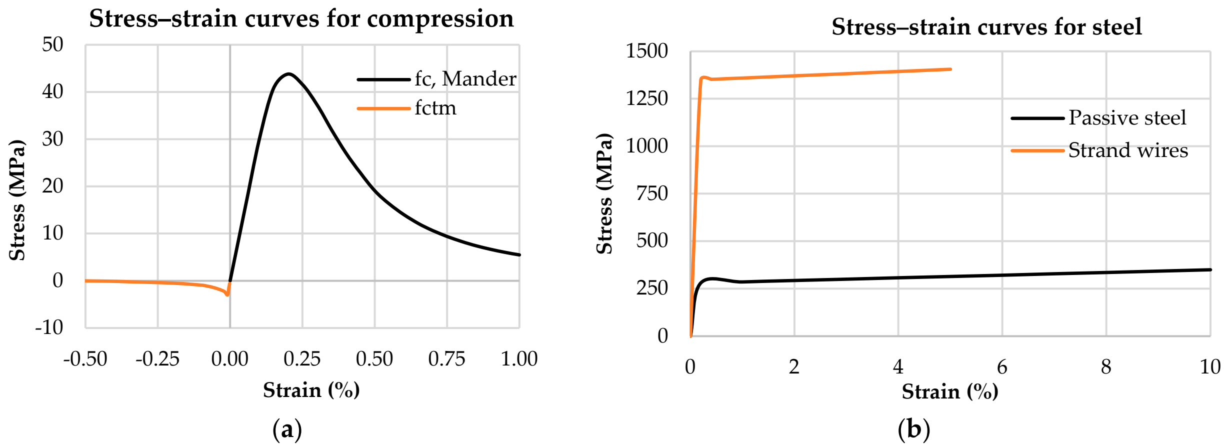

Figure 14. Stress–strain curves adopted in simulations: (**a**) concrete compressive and tensile stress–strain curves (fctm is the tensile strength of concrete); (**b**) post-tensioning and passive reinforcing steel curves.

3.6.2. Post-Processing

The processing of boundary conditions consisted of two phases. The first phase induced the prestressing forces in the column wall simultaneously with service loads under normal-day operation. Once convergence was reached, the second phase was initiated by increasing the surface pressure until failure. Two models were processed: one in which 100% of the prestressing forces were induced by the predefined field and another without prestressing forces induced by the predefined field. In other words, one model simulated the effects of prestressing and the other did not. Since both models exhibited similar mechanical failure modes, differing only in ultimate strength and ductility capacities, only the results of the model without prestressing forces are presented. The capacity curves of these models are shown at the end of this section.

The first observation made when assessing the stress gradient across the column-wall element is that the stress path was transmitted through a tied-arch mechanism rather than a beam effect, as shown in Figure 15a. In this situation, strain distributions might be highly nonlinear, and the section may not remain plane, meaning that classical linear elastic bending theory could be invalid. In the same figure, it can be seen that the stresses at the top chord of the cross-beam exceeded the lower-bound tensile strength of the concrete. Another observation was the development of permanent plastic strain within the critical section (starting at the top cross-beam chord and propagating toward the bottom chord, where there is a geometric shift) once the tensile strength thresholds were exceeded (Figure 15b).

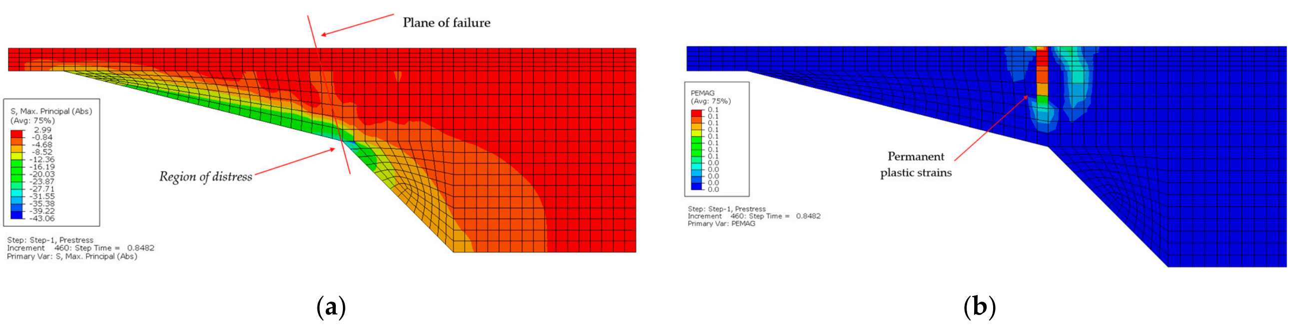

Figure 15. Model without prestressing forces in post-processing (undeformed shape): (**a**) stress distribution across column-wall depth; (**b**) permanent plastic strain distribution in critical section.

Since the concrete at the critical section cracked, large quantities of unbalanced stress were transferred to the steel through the embedded property. This activated a ductile response in the section by inducing strain in the steel rebars. If sufficient intrinsic ductility capacity was available, large-section cracking and deformation would be expected. This ductility capacity was mostly related to the amount and quality of reinforcement within the critical section. Accordingly, the model could reach the yielding limit and even undergo strain hardening for both the prestressing strands and the passive steel, as shown in Figure 16a. This occurred simultaneously with extensive cracking within the critical section, as shown in Figure 16b. After that, a plastic hinge developed at the top chord of the cross-beam and propagated almost entirely through the depth of the column-wall extension.

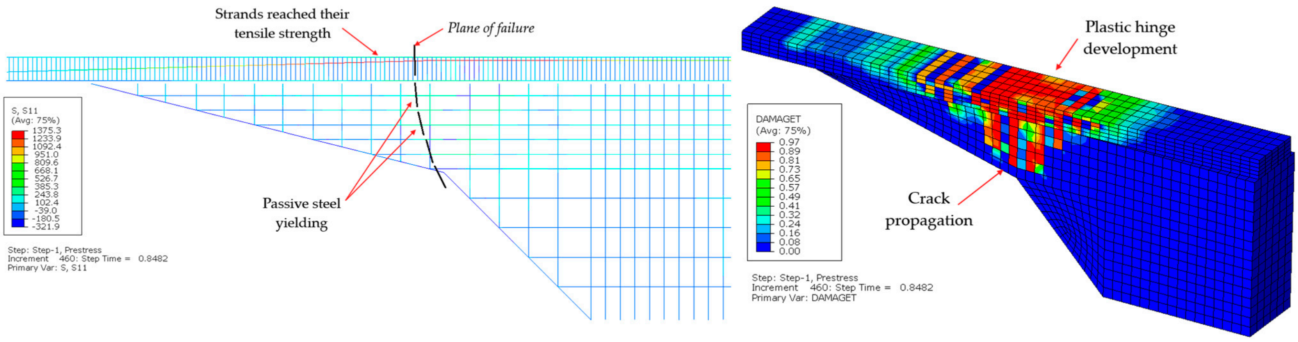

(**a**) (**b**)

Figure 16. Model without prestressing forces in post-processing (undeformed shape): (**a**) stresses in reinforcing steel; (**b**) concrete damage plasticity (CDP) model with crack propagation.

The preceding figures suggest that the modeling technique employed could effectively capture the failure mode observed, summarized as follows: the failure initiated during bending, with crack propagation throughout the entire depth of the column-wall extension. This was followed by the yielding of the flexural reinforcement and the formation of a plastic hinge in the cross-beam. Once this mechanism developed, extensive cracking and deformation would have been expected, and without proper reinforcement detailing, the section would shear off.

3.6.3. Numerical Strength

The ductility capacity and strength of the column-wall extension were measured in terms of the vertical deformation of the cross-beam tip end and the corresponding shear load, obtained from the numerical model outputs. Shear loads were calculated from the column-wall reaction force, and the results are shown in Figure 17 for both models with and without prestressing forces. Also, the results can be compared with the estimated shear demand (manually calculated) and the shear demand to reach the full theoretical flexural capacity of the section (theoretical beam flexural strength). This estimation is based on the overall structural dead load and vehicle traffic loads (discussed in Section 3.4), excluding the column self-weight beyond the critical section.

Figure 17 suggests that the numerical model was able to withstand the prescribed load demand recommended by the former Brazilian standard for both models with and without prestressing. In both cases, yielding was initiated after the beam-end deflection exceeded 25 mm (0.3% drift), with the model without prestressing exhibiting lower strength during the post-elastic regime. In addition, prestressing forces induced an upward beam deflection (negative, since the positive reference is downward), which was eventually counteracted by the increasing surface pressure over the cross-beam. The prestressing model showed higher capacity and similar ductility, as both strengths increased due to the steel strain-hardening property. This assessment indicates that the structural design might have been adequate for the load demand during the construction period and even for modern demands. However, since the viaduct collapsed suddenly (brittle failure), the structure may have lost part of its ductility capacity over time, as evidenced by the observations in Section 3.2. When the dashed lines meet the solid capacity curve lines, failure could have occurred at a small deformation demand (under 25 mm), indicating little available ductility. This suggests that material degradation coupled with a loss of ductility (due to a reduction in steel areas and stress corrosion) might have triggered the collapse mechanism rather than excess load or poor engineering judgment.

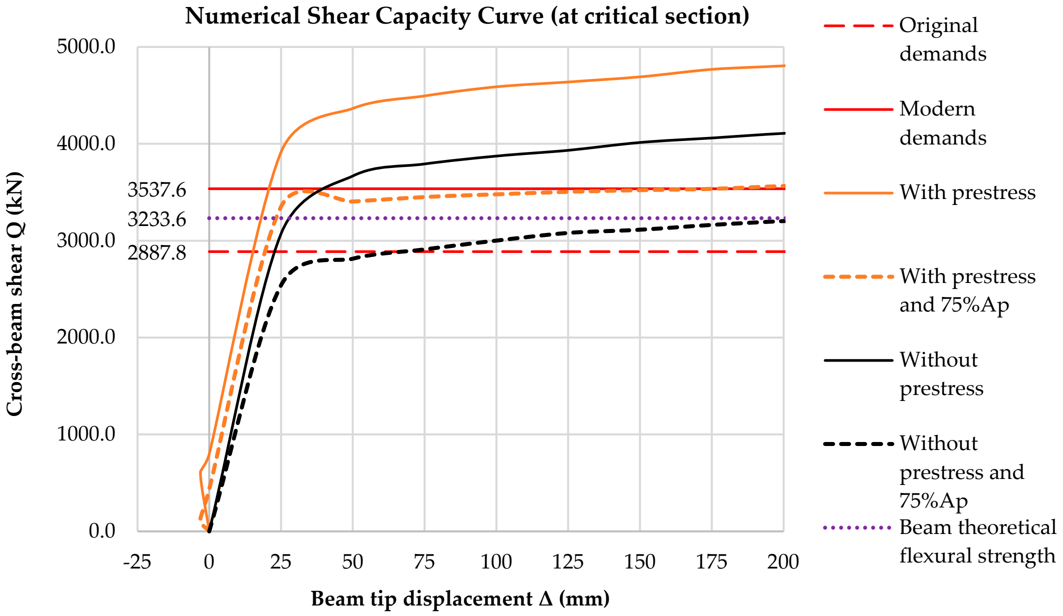

Figure 17. Capacity curves of numerical models with and without prestressing forces.

After this assessment, two other models were simulated to account for the degradation of mechanical properties. In this situation, the corrosion of strands was considered for both models, which was conveniently introduced into the models by the deliberate reduction of the active steel areas of the wires. A reduction of 25% in Ap was induced for both models, with and without the effects of prestress. Since the manual calculations in Section 3.5 suggested a reduction of three cables (around 19% reduction), the 25% value resulted in models with slightly lower strengths than demands and was within the 50% steel area loss reported in Section 3.2. The results are shown by the dashed lines in Figure 17, which tend to overlap the original and modern demands: the degraded curves plateau below the modern demand of 3537.6 kN but above the original 1960 demand of 2887.8 kN, *strongly suggesting that the degraded section could still satisfy the loads it was designed for in 1960 but could no longer satisfy contemporary demands*. This confirms the hypothesis that corrosion of strands reduced capacities to lower safety levels, which are quantitatively evaluated here.

3.6.4. Further Comments on Modeling

It is important to note that the numerical model had idealized assumptions that could result in higher strength and ductility than the actual prestressed column-wall extension could have exhibited. The assumption that there is a perfect bond between steel and concrete may not be valid, as the asset was built with smooth reinforcing steel. The use of these rebars tends to alter the mechanical behavior of concrete sections due to bond slip, intensifying inelastic response. Older structures built with smooth bars tend to develop higher chord rotations at member ends and reduced energy dissipation and to concentrate damage (usually single large cracks) in plastic hinges rather than well-distributed, densely spaced thin cracks [33]. This can alter the strength, deformation capacity, and failure mechanisms of RC elements, particularly for specimens subjected to cyclic loads [34]. Since site investigations revealed a large individual crack (Figure 9a) rather than well-distributed cracks, this evidence supports the previous comments.

Another possible increase in apparent ductility might be related to the rocking mechanism associated with unbonded reinforcement: the opening of large cracks due to bond slip and concrete softening at the member-end reaction can increase deformation capacity [35]. This can be seen in the large crack that developed in the critical section and the concentrated compressive stress in the bottom chord (Figure 15a). This phenomenon prevents the development of complete flexural behavior of the element made with smooth bars compared to members with deformed bars [36]. In other words, RC members with these characteristics might fail before developing full flexural strength.

While the numerical capacity curve (Figure 17) provides a valuable baseline for evaluating the structure's intended performance, the assumption of a perfect bond between the concrete and the smooth reinforcing bars overestimates the available ductility and stiffness at the ultimate limit state. This can be seen in the strain-hardening behavior reaching higher levels compared to the demands. Rather than invalidating the flexural mechanisms identified by the model, this limitation reinforces the forensic findings. The true structural capacity should be lower than the idealized models suggest; the bond-slip degradation acted as an important aggravating factor that curtailed theoretical ductility and possibly contributed to the viaduct's sudden, brittle collapse observed on site. However, since bond-slip modeling would provide no basis for validating the simulation, introducing corrosion by deliberately reducing the active steel area was considered practical.

In addition, the model adopted for the manual calculations was based on beam flexural theory, which might deviate from the actual structural behavior of the viaduct, which is characterized by large-volume sections. In addition to differences in actual prestress loss, this could lead to variations in the structural response during capacity estimation. Nonetheless, the meticulous numerical representation of the asset remains secondary in this manuscript since validation is not possible. The main idea behind its numerical calculation was to determine the level of understanding of the structure's response based on the original design.

Lastly, the type of technology available at the time (such as the use of smooth reinforcement, low concrete compressive strength, small amounts of longitudinal and transverse reinforcement, normal-relaxation strands, and increased cyclic demands) could have impacted the long-term response. These points are discussed in detail in the next section.

4. Failure Diagnostics

4.1. Shear and Flexural Failure Theory for Structural Concrete

The ultimate shear-carrying capacity of slender, prismatic reinforced concrete (RC) members is fundamentally governed by an interactive combination of concrete and steel shear-transfer mechanisms. This multi-component system comprises the intrinsic shear strength of the uncracked cementitious matrix, aggregate interlock along crack planes, the dowel action of longitudinal reinforcement, and the tensile resistance of transverse reinforcement. The allocation of the total shear demand among these mechanisms is highly dependent on the evolving strain field and localized structural kinematics. For instance, during the propagation of diagonal tension cracks (a result of combined flexural and shear stresses), crack opening induces interface sliding and separation, thereby degrading the frictional efficiency of aggregate interlock. Conversely, the introduction of prestressing forces establishes a compressive state that confines these shearing interfaces, significantly amplifying their effective shear-transfer resistance. Under conditions of net axial tension or cyclic loading, the contact zones undergo severe mechanical friction, reducing the interface's internal frictional resistance due to wear.

In conventionally reinforced concrete members, escalating shear deformations prompt a critical redistribution of internal forces. As the aggregate interlock mechanism undergoes degradation, the shear demand is transferred to the remaining active components: the dowel action of the longitudinal reinforcement, the intrinsic shear capacity of the concrete compressive zone, and the tensile resistance of the stirrups. Under monotonically increasing loads, the ultimate limit state is typically reached when the transverse reinforcement yields, triggering a failure in which the remaining shear-transfer mechanisms are exhausted quasi-simultaneously. Quantitatively, the magnitudes of the dowel, stirrup, and concrete shear components are explicitly coupled to the geometric reinforcement ratios and the constitutive material strengths of both phases. Crucially, longitudinal reinforcement provides an essential layer of structural redundancy beyond its pre-peak shear contribution. Following localized concrete macro-cracking, the dowel action transitions into a critical suspension mechanism, mitigating sudden progressive collapse by physically anchoring the detached structural segments (a structural redundancy principle).

Under cyclic loading, the efficiency of individual shear-resisting components is severely compromised by the evolution of damage. This degradation is characterized by widespread micro-cracking within the concrete and plastic strain accumulation in the steel, which collectively diminish individual material resistances.

Additionally, in stirrup-deficient elements subjected to high shear demands, the structural response differs drastically from that of standard RC elements. Here, the failure morphology is explicitly coupled to the elastic stability of the dowel action. Once the longitudinal reinforcement transitions into the post-yield regime, the structural system lacks alternative internal load paths, thereby transferring the entire strain demand to the concrete. This induces a high concentration of stress, resulting in a brittle mechanism and sudden failure. Furthermore, elements lacking transverse steel are highly vulnerable to size effects; as structural dimensions increase, localized stress concentrations intensify, leading to a marked reduction in apparent shear strength. In contrast, the introduction of transverse reinforcement provides a critical crack-bridging mechanism that neutralizes size-effect degradation [27].

For flexural failures, on the other hand, when RC systems have sufficient ductility capacity, ultimate limit states tend to be reached with considerable warning, typically represented by large deformations coupled with widespread cracking. The flexural capacity of prismatic RC members presumes equal strain deformations of concrete and steel (or perfect bond), as the latter starts to deform once the concrete cracks. In this way, the force equilibrium of the section is determined considering that both elements reach their design strength simultaneously. When the bond between steel and concrete deteriorates due to excessive cracking or cyclic loading, there is unequal force participation in attaining section equilibrium, so the concrete (compressive block) needs to develop higher forces to maintain balance. Depending on the strain state of the concrete and the position of the section neutral axis, this may not be possible, culminating in crushing failure of the concrete, which can occur even before the steel reaches the post-yield state [37].

Lastly, for prestressed concrete prismatic elements, steel actively increases both the flexural and shear resistance of members by inducing a deliberate state of compression. However, the prestressing steel is highly sensitive to corrosion under constant pre-elongation (stress corrosion). For stress values exceeding 50% of the steel's strength, stress corrosion drastically degrades the ductility of the element (embrittlement), and failure is typically brittle, often associated with little or no loss of metal, possibly without structural warning. For post-tensioned bonded tendons, the most critical factors are the type and quality of the grout and the grouting operation. In structures where poor practices result in voids in the encapsulation of wires within strands, the bundling of wires can result in sudden fracture after stress corrosion. Projects with good-quality isolation and adequate materials and techniques have been observed to be trouble-free [38]. On the other hand, if stress corrosion triggers the failure of prestressing strands in large concrete structures, severe failure can occur due to large unbalanced forces, even under service loads.

4.2. The Viaduct Failure Explained

Forensic analysis suggests that the partial collapse originated from the tension-assisted corrosion of the prestressing strands within the support cross-beams at the pier caps. The structural morphology of the key-closure encasement over the cross-beam served to conceal this localized deterioration, obstructing direct visual diagnostic pathways to this fracture-critical component. The evidence of poor wire isolation within the metal tubes suggests poor grout injection during construction, as shown in Figure 10. Also, environmental degradation could have been accelerated by chronic moisture infiltration through road deck cracks, unforeseen cyclic loading demands, and inadequate maintenance throughout the bridge lifecycle. These variables most likely degraded the prestressing wires, which were essential components of the load-balancing system, since the extension cross-beam was operating as a cantilever. This hypothesis is supported by evidence from the manual determination of strengths and demands and by numerical modeling. Structural analysis indicated that the viaduct design had sufficient strength and ductility, despite the low steel reinforcement ratios. Thus, most likely, the materials lost ductility over time or the wires lost significant effective steel area, which made it possible for a critical plastic hinge to develop within the prestressing cross-beam.

After the triggering of the flexural mechanism, the system was incapable of developing alternative load paths due to limited passive reinforcement (lack of structural redundancy). Had structural redundancy been available, supplementary passive steel would have provided post-peak load paths via dowel action, helping to prevent catastrophic collapse after matrix fracture. This behavior was observed on site during the debris investigation (Figure 11b) and is consistent with the manual calculations of the dowel action strength in Section 3.5. Once the plastic hinge developed, the section failed suddenly in shear, making it incapable of carrying the unbalanced loads of the system.

These detailing flaws, in addition to time-degrading components, probably became design vulnerabilities that went undetected by municipal asset managers—a problem compounded by the absence of historical design documentation, conceptual design, advanced structural aging, and the outdated code applicable during the period of construction.

Post-failure forensic investigation enabled consistent mapping of the rupture plane and detailed characterization of the steel configuration within the column-wall cross-beam extension, as depicted in Figure 3. In summary, the viaduct failure was probably the mechanical realization of long-term systematic vulnerabilities, which can be synthesized into a combination of six core problems:

1. **Attenuation of Prestressing Forces via Steel Stress Corrosion**: The structural capacity of the critical section was probably compromised by the mechanical degradation of the high-strength strands via tension-assisted corrosion. Moisture infiltration through road surface fissures and high cyclic demands possibly initiated localized steel pitting that culminated in ductility/strength losses. This reduced the prestressing forces balancing the cantilever column-wall extension, causing an immediate deficit in flexural, shear, and ductility capacity.
2. **Deficient Structural Redundancy and Scale-Dependent Shear Resistance**: The lack of structural redundancy prevented the section from developing alternative load paths, specifically due to the limited passive longitudinal steel within the critical section. This deficiency prevented the activation of effective dowel action needed

to prevent progressive collapse. Furthermore, the lack of transverse reinforcement hoops within the critical cross-section over the overall depth of the column wall prevented localized crack confinement, inducing size effects that compromised the shear resistance.

3. **Concealed Geometry and Lost Documentation**: Critical engineering diagnostic pathways were seriously obstructed by architectural and infrastructural configurations. The integration of structural infills, drainage conduits from adjacent commercial facilities, and non-removable cast-in-place concrete joints physically concealed the core post-tensioning elements from non-destructive visual evaluation. This lack of physical accessibility, compounded by the loss of original engineering drawings and historical archives, prevented proper monitoring of active crack propagation and internal leaching.
4. **Poor Material Quality and Detailing**: The older materials exhibited low-performance characteristics compared to modern design standards, deviating from contemporary requirements. The use of smooth, non-deformed passive reinforcing bars impaired bond-slip performance, while the use of rounded alluvial gravel compromised the concrete shear strength. Also, modern heavy-vehicle load spectra could have limited aggregate interlock efficiency and overall shear capacity.
5. **Unpredicted Historical Amplification of Cyclic Fatigue**: The viaduct underwent cyclic loading that probably exceeded the design-life envelopes expected during the construction period in Brasilia. Estimates of modern design loads could have been 22.5% higher than the original demands defined by older revisions of the Brazilian standard. And the loading frequency could have been substantially higher than originally anticipated, thus increasing susceptibility to cyclic fatigue.
6. **Long-Term Rheological Phenomena**: While time-dependent variables (steel stress relaxation and concrete creep) were omitted from the primary forensic assessment, their contributions possibly influenced material performance over the asset's lifespan. However, their role in time-dependent material decay within the global failure envelope remains secondary, since their effects are difficult to estimate accurately. Their impact on structural capacity was possibly far less critical than the compounding effects of cyclic deterioration and the intrinsic shear detailing deficiencies.

5. Viaduct Strengthening and Retrofitting

Following the emergency stabilization of the viaduct through shoring and continuous monitoring, long-term structural recovery techniques, such as structural strengthening and repairs, were implemented. They focused on replacing failed components and enhancing the remaining structure to provide adequate performance. The overall detailing is shown in Figure 18. The authors of this research had access to the project documentation and detailed design drawings, which are briefly described in this manuscript, and also held meetings with the lead engineer, Bruno Contarini, the engineer who designed the original viaduct.

For the column-wall cantilever extensions, the prestressed cross-beam was removed and reconstructed to meet current standard requirements. The new cross-beams featured sufficient prestressing and non-prestressing steel, as well as modern bearing pads, to support the road deck. Where the partial collapse occurred, the full deck segment was demolished, and a new deck with similar engineering characteristics, made of prestressed beams and a concrete slab, was designed under the elastic regime and built. This new design considered modern load demands, previously mentioned in this manuscript.

https://doi.org/10.3390/buildings16193806

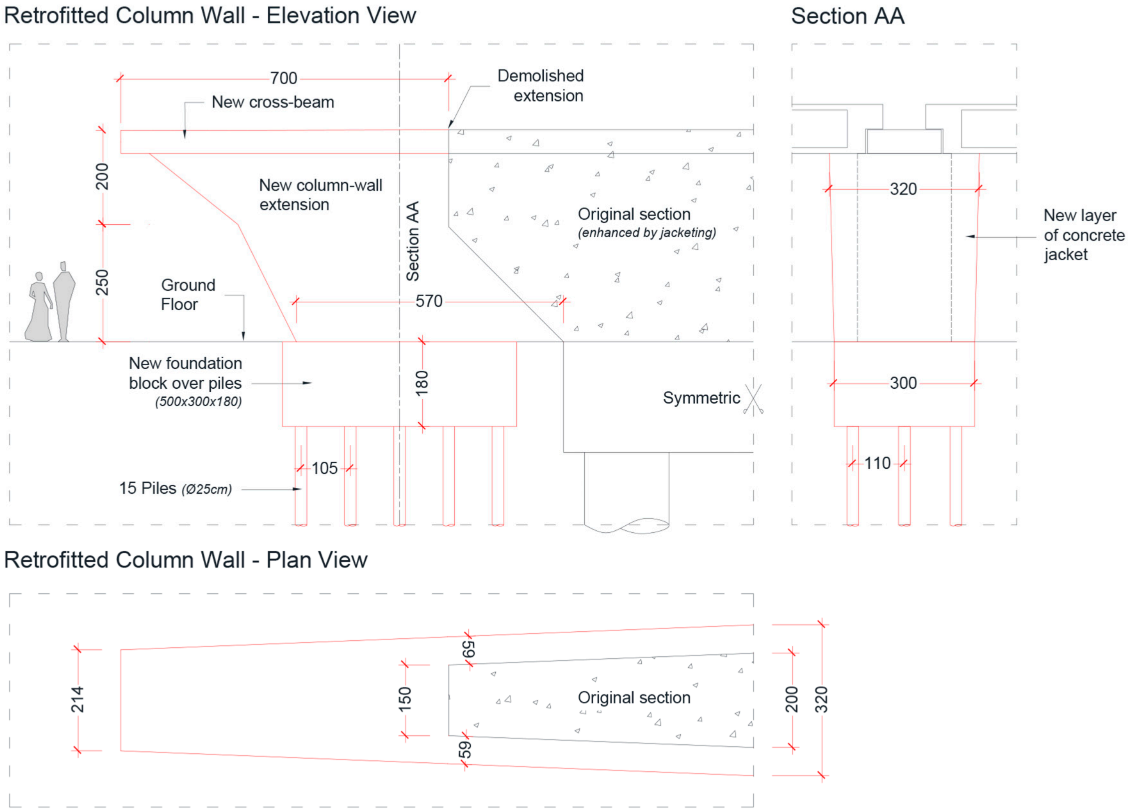

Figure 18. Engineering solution employed for the retrofit of the asset, by concrete jacketing and construction of a new foundation block (both in red lines). Units are in cm, and dimension lines in red.

The solution employed consisted of demolishing the extensions of the column walls and replacing them with a new column-wall section that encapsulated the former concrete wall. This section enhancement was achieved by concrete jacketing with prestressing ties to greatly increase its load-bearing capacity. The overall column width was increased from 200 cm to 320 cm, and the new section incorporated large amounts of passive reinforcing steel compared to the original design. The corroded column rebars were treated and protected with the new layer of confined reinforced concrete and sufficient concrete cover. Also, beneath the new extension walls, massive foundation blocks (500 cm × 180 cm × 300 cm) supported on 15 piles were implemented. Likewise, to create an adequate bonding surface between the old and new concrete, reinforcing ties were uniformly distributed around the old column perimeters and attached to them using chemical adhesives. The final view of the retrofitted asset is indicated in Figure 19.

To prevent the chronic water infiltration that caused the original corrosion, the gap between slabs above the column walls at the cross-beam interface was sealed with precast concrete pieces as structural joints, which would permit access for maintenance. This was a key repair requirement that enabled direct visual inspection of the bearing pads and support elements at a reasonable cost, a feature missing from the original 1960 design. The final goal of these combined techniques was to ensure a residual service life of at least 100 years for the recovered structure—reflecting a prescriptive design target based on the NBR 6118 design specifications for concrete and steel (including design tolerances, minimum cover, adequate construction protocols and practices, standardized materials, etc.). The strengthening and retrofitting of the asset took about 16 months to complete, and the viaduct was reopened on 4 June 2019. Further in-depth information on the retrofitting implementation, details, and process can be found in [13].

(a) (b)

Figure 19. Viaduct after retrofitting: (**a**) view of the new jacketed column wall; (**b**) removal of the restaurant and integration with the new park.

6. Lessons from the Rubble

The political challenge of building Brasília within a compressed four-year timeline significantly accelerated infrastructure development, deeply testing the engineering community during a period marked by scarce regulatory and material resources. Consequently, the pioneering deployment of post-tensioned bridge systems, coupled with highly uncertain long-term traffic forecasting, may have introduced hidden vulnerabilities across analogous structures in the city, as this work consistently demonstrated through the forensic investigation of the South Road Axis Viaduct collapse.

This investigation isolated six possible interconnected factors, which most likely governed the failure of the viaduct: material degradation compounded over time (chronic water infiltration, poor construction execution, and material rheological degradation); deficient structural redundancy (not required by outdated standards); architectural and structural configurations that precluded routine maintenance and early damage detection; sub-optimal material properties and poor execution protocols (alluvial concrete aggregates, smooth reinforcing bars, and extensive ungrouted post-tensioning voids); and unpredicted, high-amplitude cyclic load spectra that probably exceeded possible projections.

Similar to the shear failure of the Wilkins Air Force Depot in Ohio (in 1955) and the Morandi Bridge collapse in 2018, assigning a single causative factor is analytically insufficient to explain the ultimate limit state of the South Road Axis Viaduct in Brasilia in 2018. While catastrophic, this partial collapse provides a useful diagnostic representation of how aging, non-conforming engineering heritage assets perform under modern structural demands, establishing a vital reference point for infrastructure engineering design and management.

7. Recommended Future Work

Among the many aspects observed in this paper related to the complexity of the South Road Axis Viaduct, the authors recommend the following points for analysis in future work:

- Comparison of the beam flexural model with the strut-and-tie model (STM) in predicting the shear strength of the critical section;
- Evaluation of bond-slip mechanics in the FE model to consider the influence of slip due to the presence of smooth reinforcement;
- Cyclic and fatigue assessment of the viaduct's main column wall to estimate structural degradation effects.

https://doi.org/10.3390/buildings16193806

Author Contributions: Conceptualization, Y.B.C.; methodology, Y.B.C. and C.F.; software, Y.B.C. and J.M.; formal analysis, Y.B.C., J.M., and H.V.; investigation, Y.B.C. and C.F.; resources, C.F.; data acquisition, C.F.; writing—original draft preparation, Y.B.C.; writing—review and editing, Y.B.C., J.M., and H.V.; supervision, J.M.; project administration, H.V. and J.M.; funding acquisition, H.V. All authors have read and agreed to the published version of the manuscript.

Funding: This work was financially supported by UID/04708/2025 (https://doi.org/10.54499/UID/04708/2025) of CONSTRUCT—Instituto de I&D em Estruturas e Construções—funded by Fundação para a Ciência e a Tecnologia, I.P./MECI, through national funds. This work was also financially supported by national funds through FCT/MCTES (PIDDAC), under project 2022.05721.PTDC, DOI: 10.54499/2022.05721.PTDC (https://doi.org/10.54499/2022.05721.PTDC).

Data Availability Statement: The original contributions presented in this study are included in the article. Further inquiries can be directed to the corresponding author.

Acknowledgments: The authors would like to thank the Nova Companhia Urbanizadora da Nova Capital (NOVACAP) for the interviews, site explorations conducted during the incident, and public documents that were essential to the theoretical basis of this paper.

Conflicts of Interest: Author Carlos Feijão was employed by the company Companhia Urbanizadora da Nova Capital do Brasil—NOVACAP. The remaining authors declare that the research was conducted in the absence of any commercial or financial relationships that could be construed as a potential conflict of interest.

Abbreviations

The following abbreviations are used in this manuscript:

RC	Reinforced concrete
ULS	Ultimate limit state
ASD	Allowable Stress Design
NBR	Norma Brasileira (Brazilian standard)

References

1. DER/DF. Volume Diário de Tráfego—Trechos Rodoviários. 2021. Available online: https://www.dados.df.gov.br/dataset/volume-diario-de-trafego-trechos-rodoviarios (accessed on 27 March 2026).
2. G1. Viaduto que Caiu no DF já Precisava de Manutenção em 2009, Diz Relatório. 2018. Available online: https://g1.globo.com/df/distrito-federal/noticia/viaduto-que-caiu-no-df-ja-precisava-de-manutencao-em-2009-diz-relatorio.ghtml (accessed on 9 November 2018).
3. Brasilia, A.D. GDF Investe 160 Milhões para Reformar 40 Viadutos e Construir Quatro Novos. 2019. Available online: https://www.agenciabrasilia.df.gov.br/w/gdf-investe-r-160-milhoes-para-reformar-40-viadutos-e-construir-quatro (accessed on 27 March 2026).
4. Anderson, B.G. Rigid frame failures. *J. Proc.* **1957**, *53*, 625–636. [CrossRef] [PubMed]
5. Elstner, R.C.; Hognestad, E. Laboratory investigation of rigid frame failure. *J. Proc.* **1957**, *53*, 637–668. [CrossRef] [PubMed]
6. Stamenkovic, H. Inflection points as statical supports are responsible for structural failure of AMC warehouse in Shelby, Ohio, 1955. *Matér. Constr.* **1977**, *10*, 375–384. [CrossRef]
7. Pinho, R.; Scattarreggia, N.; Orgnoni, A.; Lenzo, S.; Grecchi, G.; Moratti, M.; Calvi, G.M. Forensic estimation of the residual capacity and imposed demand on a ruptured concrete bridge stay at the time of collapse. *Structures* **2023**, *55*, 1595–1606. [CrossRef]
8. Zucca, M.; Tattoni, S.; Castri, M.D.; Simoncelli, M. On the collapse of a post-tensioned reinforced concrete truss bridge during the construction phases. *Eng. Fail. Anal.* **2024**, *158*, 107999. [CrossRef]
9. *NBR 7188*; Carga Móvel Rodoviária e de Pedestres em Pontes, Viadutos, Passarelas e Outras Estruturas. Associação Brasileira de Normas Técnicas: Rio de Janeiro, Brazil, 2013.
10. *NBR 7187*; Projeto de Pontes, Viadutos e Passarelas de Concreto. Associação Brasileira de Normas Técnicas: Rio de Janeiro, Brazil, 2021; p. 11.
11. *NBR 6118*; Projeto de Estruturas de Concreto-Procedimento. Associação Brasileira de Normas Técnicas: Rio de Janeiro, Brazil, 2025.
12. Dassault Systèmes Simulia, I. *Abaqus/CAE, Version 2023*; Dassault Systèmes Simulia, Inc.: Providence, RI, USA, 2023.

13. Galimi, S.; Pantoja, J.D.C.; Buzar, M.A.R.; Machado, P.R.S. Retrofit em obras tombadas de infraestrutura urbana: O caso do Viaduto sobre a Galeria dos Estados. *Paranoá Cad. Arquitetura Urban.* **2020**, *26*, 140–156. [CrossRef]
14. NBR *7680*; 2015 Concreto-Extração, Preparo, Ensaio e Análise de Testemunhos de Estruturas de Concreto-Parte 1: Resistência à Compressão Axial. Associação Brasileira de Normas Técnicas: Rio de Janeiro, Brazil, 2015.
15. NBR *6349*; 2008 Barras, Cordoalhas e Fios de Aço para Armaduras de Protensão—Ensaio de Tração. Associação Brasileira de Normas Técnicas: Rio de Janeiro, Brazil, 2008.
16. *NBR 6892*; 2002 Materiais Metálicos-Ensaio de Tração à Temperatura Ambiente. Associação Brasileira de Normas Técnicas: Rio de Janeiro, Brazil, 2002.
17. *ISO 15630-1*; 2010 Steel for the Reinforcement and Prestressing of Concrete—Test Methods—Part 1: Reinforcing Bars, Wire Rod and Wire. International Organization for Standardization: Geneva, Switzerland, 2010.
18. Universidade de Brasília (UnB). *RELATÓRIO TÉCNICO–Dept. ENC/UnB 001*; UnB: Brasilia, Brazil, 2018.
19. NOVACAP. *RELATÓRIO TÉCNICO-Grupo de Trabalho Conforme Decreto n. 38.841 de 06.02.2018*; Governo do Distrito Federal: Brasília, Brazil, 2018.
20. *NBR 7197*; Projeto de Estruturas de Concreto Protendido, Procedimento. Associação Brasileira de Normas Técnicas: Rio de Janeiro, Brazil, 1987.
21. *NB-1/1960*; Cálculo e Execução de Obras de Concreto Armado. Associação Brasileira de Normas Técnicas: Rio de Janeiro, Brazil, 1960.
22. *NB-2/1961*; Cálculo e Execução de Pontes de Concreto Armado. Associação Brasileira de Normas Técnicas: Rio de Janeiro, Brazil, 1961.
23. *NB-6/1960*; Cargas Móveis em Pontes Rodoviárias. Associação Brasileira de Normas Técnicas: Rio de Janeiro, Brazil, 1960.
24. Langendonck, T.V. *Cálculo de Concreto Armado-Vol I*; Associação Brasileira de Cimento Portland: Rio de Janeiro, Brazil, 1959.
25. Langendonck, T.V. *Cálculo de Concreto Armado-Vol II*; Associação Brasileira de Cimento Portland: Rio de Janeiro, Brazil, 1959.
26. *EN 1992-1-1*; 2023 Eurocode 2-Design of Concrete Structures-Part 1-1: Genral Rules and Rules for Buildings, Bridges and Civil Engineering Structures. European Committee for Standardization: Brussels, Belgium, 2023; p. 408.
27. Wight, J.K.; MacGregor, J.G. *Reinforced Concrete Mechanics & Design*; Prentice Hall: Upper Saddle River, NJ, USA, 2012.
28. Rasmussen, B.H. The carrying capacity of tranceversely loaded bolts and dowels embedded in concrete. *Bygings Statiske Meddelser* **1963**, *34*.
29. Mattock, A.H.; Hawkins, N.M. Shear transfer in reinforced concrete—Recent research. *Pci J.* **1972**, *17*, 55–75. [CrossRef]
30. Vintzēleou, E.; Tassios, T. Mathematical models for dowel action under monotonic and cyclic conditions. *Mag. Concr. Res.* **1986**, *38*, 13–22. [CrossRef]
31. Mander, J.B.; Priestley, M.J.N.; Park, R. Theoretical stress-strain model for confined concrete. *J. Struct. Eng.* **1988**, *114*, 1–23. [CrossRef]
32. Cornelissen, H.A.; Hordijk, D.A.; Reinhardt, H.W. Experimental determination of crack softening characteristics of normalweight and lightweight concrete. *Heron* **1986**, *31*, 45–56.
33. Verderame, G.M.; Fabbrocino, G.; Manfredi, G. Seismic response of r.c. columns with smooth reinforcement. Part I: Monotonic tests. *Eng. Struct.* **2008**, *30*, 2277–2288. [CrossRef]
34. Opabola, E.A.; Elwood, K.J.; Oliver, S. Deformation capacity of reinforced concrete columns with smooth reinforcement. *Bull. Earthq. Eng.* **2019**, *17*, 2509–2532. [CrossRef]
35. Paderno, A.; Pelucco, S.; Metelli, G.; Preti, M. Analytical and numerical modelling of existing RC frames with smooth rebars. *Eng. Struct.* **2021**, *249*. [CrossRef]
36. Khanmohammadi, M.; Arabpanahan, M. Analyzing Seismic Response of Concrete Columns Reinforced by Plain Bars using Behavioral Mechanics. *J. Earthq. Eng.* **2019**, *23*, 1318–1345. [CrossRef]
37. Paulay, T.; Park, R.; Preistley, M. Reinforced concrete beam-column joints under seismic actions. *J. Proc.* **1978**, *75*, 585–593. [CrossRef] [PubMed]
38. Schupack, M.; Suarez, M.G. Some recent corrosion embrittlement failures of prestressing systems in the United States. *PCI* **1982**, *27*, 38–55. [CrossRef]